



# Synthesis, characterization, DNA binding and catalytic activities of Ru(III) complexes



A.Z. El-Sonbati, A.F. Shoair, A.A. El-Bindary\*, M.A. Diab, A.S. Mohamed<sup>1</sup>

Chemistry Department, Faculty of Science, Damietta-University, Damietta 34517, Egypt

## ARTICLE INFO

### Article history:

Received 26 April 2015

Received in revised form 2 June 2015

Accepted 5 June 2015

Available online xxxx

### Keywords:

Ru(III) complexes  
Molecular structure  
DNA binding  
Catalytic activities

## ABSTRACT

A new series of azo dye ligands 4-(4-hydroxy-5-(aryldiazenyl)-2-thioxothiazol-3(2H)-yl)benzenesulfonamide (HL<sub>n</sub>) were synthesized by the coupling of 3-sulfamoylphenylrhodanine with aniline and its *p*-derivatives. These ligands and their Ru(III) complexes of the type *trans*-[Ru(L<sub>n</sub>)<sub>2</sub>(bipy)]Cl were characterized by elemental analysis, IR, <sup>1</sup>H NMR and UV–Visible spectra as well as magnetic and thermal measurements. The molar conductance measurements proved that all the complexes are electrolytes. IR spectra show that the ligands (HL<sub>n</sub>) act as a monobasic bidentate ligand by coordinating *via* the nitrogen atom of the azo group (—N=N—) and oxygen atom of the deprotonated —OH group of the rhodanine moiety, thereby forming a six-membered chelating ring and concomitant formation of an intramolecular hydrogen bond. The molecular and electronic structures of the ligands (HL<sub>n</sub>) were also studied using quantum chemical calculations. The calf thymus DNA binding activity of the ligands (HL<sub>n</sub>) was studied by absorption spectra measurements. The Ru(III) complexes were tested as a catalysts for the dehydrogenation of benzylamine to benzonitrile with *N*-methylmorpholine-*N*-oxide as co-oxidant at room temperature.

© 2015 Elsevier B.V. All rights reserved.

## 1. Introduction

Rhodanine (2-thioxothiazolidine-4-one) derivatives are a good series of ligands capable of binding metal ions leading to metal complexes with increasing properties. Efforts have been made to carry out detailed studies to synthesize and to elucidate the chemical structural and electronic properties of novel families of complexes with rhodanine derivatives as a novel chelating bidentate azo dye models [1–4]. Azo compounds consist of at least a conjugated chromophore azo (—N=N—) group in association with one or more aromatic or heterocyclic system. Commercially, these colorants are the largest and most versatile class of organic dyestuffs [5]. The design, synthesis and structural characterization of azo dye complexes are a subject of current interest due to their structural, magnetic and spectral properties [6]. The widest usage of the azo dyes is due to the number of the variations in the chemical structure and the methods of application which are generally not complex. Aryl azo pyridine dyes generally have a high molar extinction coefficient, medium to high light and wash fastness properties [7]. In recent years, azo dyes have attracted wide interest and found many uses in various fields such as dyeing of textile fibers, coloring of different materials, biological–medical studies, organic synthesis and advanced applications including optical storage capacity, optical switching, holography and non-linear optical properties [8,9]. Azo

compounds and their metal complexes are known to be involved in a number of biological reactions, such as inhibition of DNA, RNA, and protein synthesis, nitrogen fixation and carcinogenesis [10].

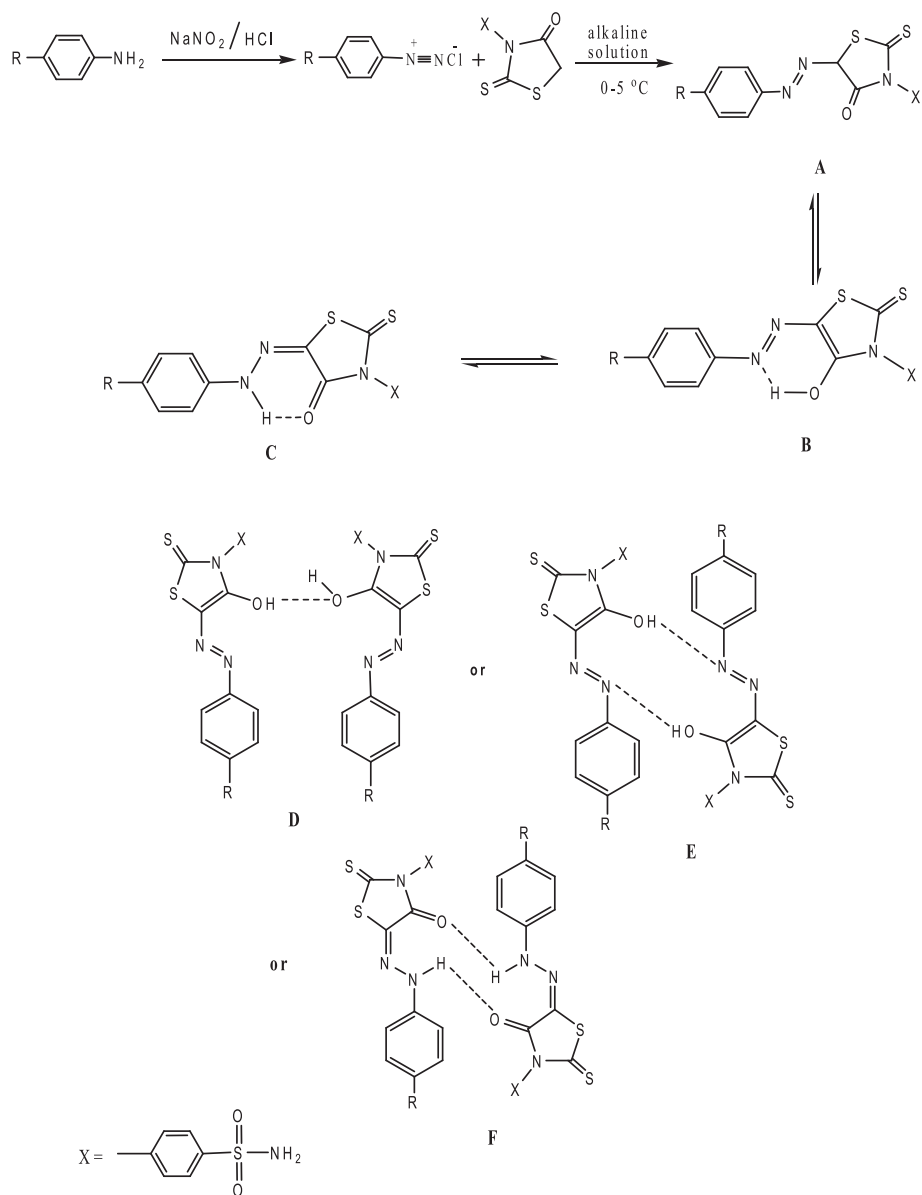
The chemistry of ruthenium complexes is of significant importance [11,12], because of the fascinating reactivities exhibited by the resultant complexes and the nature of the ligands that dictates the property of those complexes. Ruthenium compounds have been the subject of great interest and impressive development in the last decades for many reasons, especially due to their catalytic [13,14] and anticancer activities [15–17]. Ruthenium generally demonstrates affinity towards *N*-donor molecules such as proteins and DNA. The mechanism of the action of antitumor-active ruthenium compounds is not entirely known. Closely, it is thought that the complexes containing chlorides, or other easily leaving group, can hydrolyze *in vivo*, allowing the covalent binding of the nucleobases from DNA to ruthenium [18]. The Ruthenium complexes have applications in the fields of biochemistry, photochemistry and photophysics [19]. The last few decades have seen an increased interest in ruthenium(II) polypyridyl complexes as building blocks in supramolecular devices due to their favorable excited state and redox properties as well as structural probes for DNA. Ruthenium complexes are also showing promising results in anti-tumor activity and they target a broad spectrum of cancers [20].

Herein, we report the synthesis and characterization of 4-(4-hydroxy-5-(aryldiazenyl)-2-thioxothiazol-3(2H)-yl)benzenesulfonamide (HL<sub>n</sub>) and their Ru(III) complexes by different spectroscopic techniques. IR spectra show that the ligands (HL<sub>n</sub>) act as a monobasic bidentate ligand by coordinating *via* the nitrogen atom of the azo group (—N=N—) and

\* Corresponding author.

E-mail address: [abindary@yahoo.com](mailto:abindary@yahoo.com) (A.A. El-Bindary).

<sup>1</sup> Abstracted from his M.Sc. Thesis.



R = -OCH<sub>3</sub> (**HL**<sub>1</sub>), -CH<sub>3</sub> (**HL**<sub>2</sub>), -H (**HL**<sub>3</sub>) and -NO<sub>2</sub> (**HL**<sub>4</sub>)

**Fig. 1.** The formation mechanism of ligands (HL<sub>n</sub>).

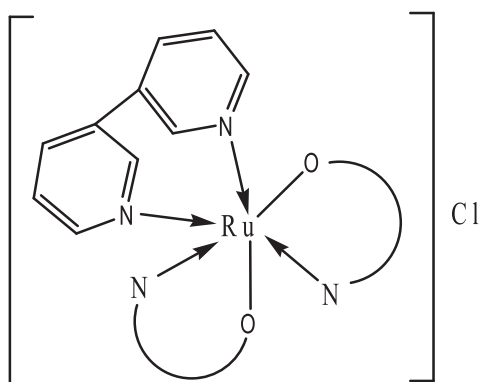


**Fig. 2.** The proposed structure of the complexes [Ru(L<sub>n</sub>)<sub>2</sub>(bipy)]Cl (**1-4**).

oxygen atom of the deprotonated —OH group of the rhodanine moiety. The calf thymus DNA binding activity of the ligands (HL<sub>n</sub>) was studied by absorption spectra measurements. The optimized bond lengths,

**Table 1**

Physical properties and elemental analysis data of the ligands (HL<sub>n</sub>) and their Ru(III) complexes (**1-4**).

Compound	Yield (%)	M.P. (°C)	% Calcd. (found)		
			C	H	N
HL <sub>1</sub>	67.07	228	45.48 (45.73)	3.33 (3.12)	13.26 (13.45)
[Ru(L <sub>1</sub> ) <sub>2</sub> (bipy)]Cl ( <b>1</b> )	67.41	>300	47.27 (47.70)	3.47 (3.60)	13.47 (13.40)
HL <sub>2</sub>	68.41	233	47.27 (47.54)	3.47 (3.64)	13.42 (13.80)
[Ru(L <sub>2</sub> ) <sub>2</sub> (bipy)]Cl ( <b>2</b> )	68.71	>300	56.55 (55.90)	3.80 (3.66)	6.60 (6.80)
HL <sub>3</sub>	71.59	218	45.89 (45.81)	3.03 (3.15)	14.27 (14.65)
[Ru(L <sub>3</sub> ) <sub>2</sub> (bipy)]Cl ( <b>3</b> )	71.90	>300	45.58 (45.01)	3.26 (3.49)	12.66 (12.5)
HL <sub>4</sub>	76.35	238	41.17 (41.27)	2.54 (2.34)	16.00 (16.24)
[Ru(L <sub>4</sub> ) <sub>2</sub> (bipy)]Cl ( <b>4</b> )	76.57	>300	41.11 (41.19)	2.57 (2.54)	14.38 (14.73)

bond angles and calculated quantum chemical parameters for the ligands ( $HL_n$ ) were investigated. The ligands considering that the phenolic —OH group may enhance their affinity towards DNA binding through formation of hydrogen bonding. The Ru(III) complexes were tested as a catalysts for the dehydrogenation of benzylamine to benzonitrile with N-methylmorpholine-N-oxide as co-oxidant at room temperature.

## 2. Materials and methods

### 2.1. Materials and apparatus

All reagents were purchased from Aldrich, Fluka and Merck and were used without any further purification. CT-DNA was purchased from SRL (India). Double distilled water was used to prepare all buffer solutions.

Microanalytical data (C, H and N) were collected on Automatic Analyzer CHNS Vario ELIII, Germany. Spectroscopic data were obtained using the following instruments: FTIR spectra (KBr discs, 4000–400  $\text{cm}^{-1}$ ) by Jasco FTIR-4100 spectrophotometer; the  $^1\text{H}$  NMR spectra by Bruker WP 300 MHz using  $\text{DMSO-d}_6$  as a solvent containing TMS as the internal standard. UV-Visible spectra by Perkin-Elmer AA800 spectrophotometer Model AAS. The molecular structures of the investigated compounds were optimized by HF method with 3-21G basis set. The molecules were built with the Perkin Elmer ChemBio Draw and optimized using Perkin Elmer ChemBio3D software [21,22]. Thermal analysis of the ligands and their Ru(III) complexes was carried out using a Shimadzu thermogravimetric analyzer under a nitrogen atmosphere with heating rate of 10  $^\circ\text{C}/\text{min}$  over a temperature range from room temperature up to 800  $^\circ\text{C}$ . Magnetic susceptibility measurements were determined at room temperature on a Johnson Matthey magnetic susceptibility balance using  $\text{Hg}[\text{Co}(\text{SCN})_4]$  as calibrant. Conductivity measurements of the complexes at  $25 \pm 1$   $^\circ\text{C}$  were determined in DMF ( $10^{-3}$  M) using conductivity/TDS meter model Lutron YK-22CT.

### 2.2. Synthesis of azo dye ligands ( $HL_n$ )

The azo dye ligands (Fig. 1), 4-(4-hydroxy-5-(aryldiazenyl)-2-thioxothiazol-3(2H)-yl)benzenesulfonamide ( $HL_n$ ) were prepared [1] by coupling of 3-sulfamoylphenylrhodanine with aniline and its *p*-derivatives. A stoichiometric amount of aniline or its *p*-derivatives (0.01 mol) in 25 mL of hydrochloric acid (0.01 mol) was added dropwise to a solution of sodium nitrite (0.01 mol) in 20 mL of water at  $-5$   $^\circ\text{C}$ . The formed diazonium chloride was consecutively coupled with an alkaline solution of 3-sulfamoylphenylrhodanine (0.01 mol). The colored precipitate, which was formed immediately, was filtered through a sintered glass crucible, washed several times with water and ethanol and dried in a vacuum desiccator over anhydrous  $\text{CaCl}_2$ . The products were purified by recrystallization from ethanol.

The resulting formed ligands are:

$HL_1 = 4-(4\text{-hydroxy-5-}((4\text{-methoxyphenyl})\text{diazenyl})\text{-2-thioxothiazol-3(2H)-yl)benzenesulfonamide.}$

$HL_2 = 4-(4\text{-hydroxy-5-}((4\text{-methylphenyl})\text{diazenyl})\text{-2-thioxothiazol-3(2H)-yl)benzenesulfonamide.}$

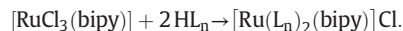
$HL_3 = 4-(4\text{-hydroxy-5-}(\text{phenyldiazenyl})\text{-2-thioxothiazol-3(2H)-yl)benzenesulfonamide.}$

$HL_4 = 4-(4\text{-hydroxy-5-}((4\text{-nitrophenyl})\text{diazenyl})\text{-2-thioxothiazol-3(2H)-yl)benzenesulfonamide.}$

### 2.3. Synthesis of Ru(III) complexes (1–4)

Ruthenium(III) complexes (Fig. 2) were synthesized according to the general procedure [23]: a stoichiometric amount of the desired ligand (0.02 mol) in ethanol (20  $\text{cm}^3$ ) was added dropwise to a hot ethanol solution (20  $\text{cm}^3$ ) of  $[\text{RuCl}_3(\text{bipy})]$  (0.01 mol) with stirring and the reaction mixture was refluxed for 3 h. The solution was

concentrated to half of its original volume by evaporation and allowed cooling at room temperature. During this, a microcrystalline solid was separated, which was isolated by filtration, washed with hot ethanol, ether and dried in a vacuum desiccator over anhydrous  $\text{CaCl}_2$ .



### 2.4. DNA binding experiments

The binding properties of the ligands to CT-DNA have been studied using electronic absorption spectroscopy. The stock solution of CT-DNA was prepared in 5 mM Tris-HCl/50 mM NaCl buffer (pH = 7.2), which a ratio of UV absorbances at 260 and 280 nm ( $A_{260}/A_{280}$ ) of ca. 1.8–1.9, indicating that the DNA was sufficiently free of protein [24], and the concentration was determined by UV absorbance at 260 nm ( $\epsilon = 6600 \text{ M}^{-1} \text{ cm}^{-1}$ ) [25]. Electronic absorption spectra (200–700 nm) were carried out using 1 cm quartz cuvettes at 25  $^\circ\text{C}$  by fixing the concentration of ligand ( $1.00 \times 10^{-3} \text{ mol L}^{-1}$ ), while gradually increasing the concentration of CT-DNA (0.00 to  $1.30 \times 10^{-4} \text{ mol L}^{-1}$ ). An equal amount of CT-DNA was added to both the compound solutions and the reference buffer solution to eliminate the absorbance of CT-DNA itself. The intrinsic binding constant  $K_b$  of the compound with CT-DNA was determined using the following Eq. (1) [26]:

$$[\text{DNA}] / (\epsilon_a - \epsilon_f) = [\text{DNA}] / (\epsilon_b - \epsilon_f) + 1 / K_b(\epsilon_a - \epsilon_f) \quad (1)$$

where  $[\text{DNA}]$  is the concentration of CT-DNA in base pairs,  $\epsilon_a$  is the extinction coefficient observed for the  $A_{\text{obs}}/[\text{compound}]$  at the given DNA concentration,  $\epsilon_f$  is the extinction coefficient of the free compound in solution and  $\epsilon_b$  is the extinction coefficient of the compound when fully bond to DNA. In plots of  $[\text{DNA}] / (\epsilon_a - \epsilon_f)$  versus  $[\text{DNA}]$ ,  $K_b$  is given by the ratio of the slope to the intercept.

### 2.5. Catalytic oxidation of benzylamine by *trans*- $[\text{Ru}(\text{L}_n)_2(\text{bipy})]\text{Cl}/\text{NMO}$

To a solution of the catalyst *trans*- $[\text{Ru}(\text{L}_n)_2(\text{bipy})]\text{Cl}$  (0.01 mmol) in 5  $\text{cm}^3$  dimethyl formamide, benzylamine (2 mmol) was added with stirring. N-methylmorpholine-N-oxide (NMO) (10 mmol) was then dissolved in DMF and the reaction mixture was further stirred for 3 h at room temperature. The mixture was reduced in vacuo and the residues were collected in diethylether, filtered through a bed of silica gel and dried over anhydrous  $\text{MgSO}_4$ . The produced benzonitrile was isolated and weighed [27].

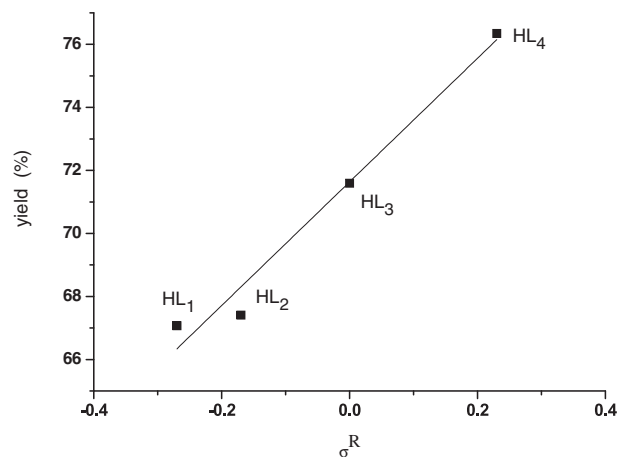


Fig. 3. The relation between Hammett's substitution coefficient ( $\sigma^R$ ) vs. yield (%) of ligands ( $HL_n$ ).

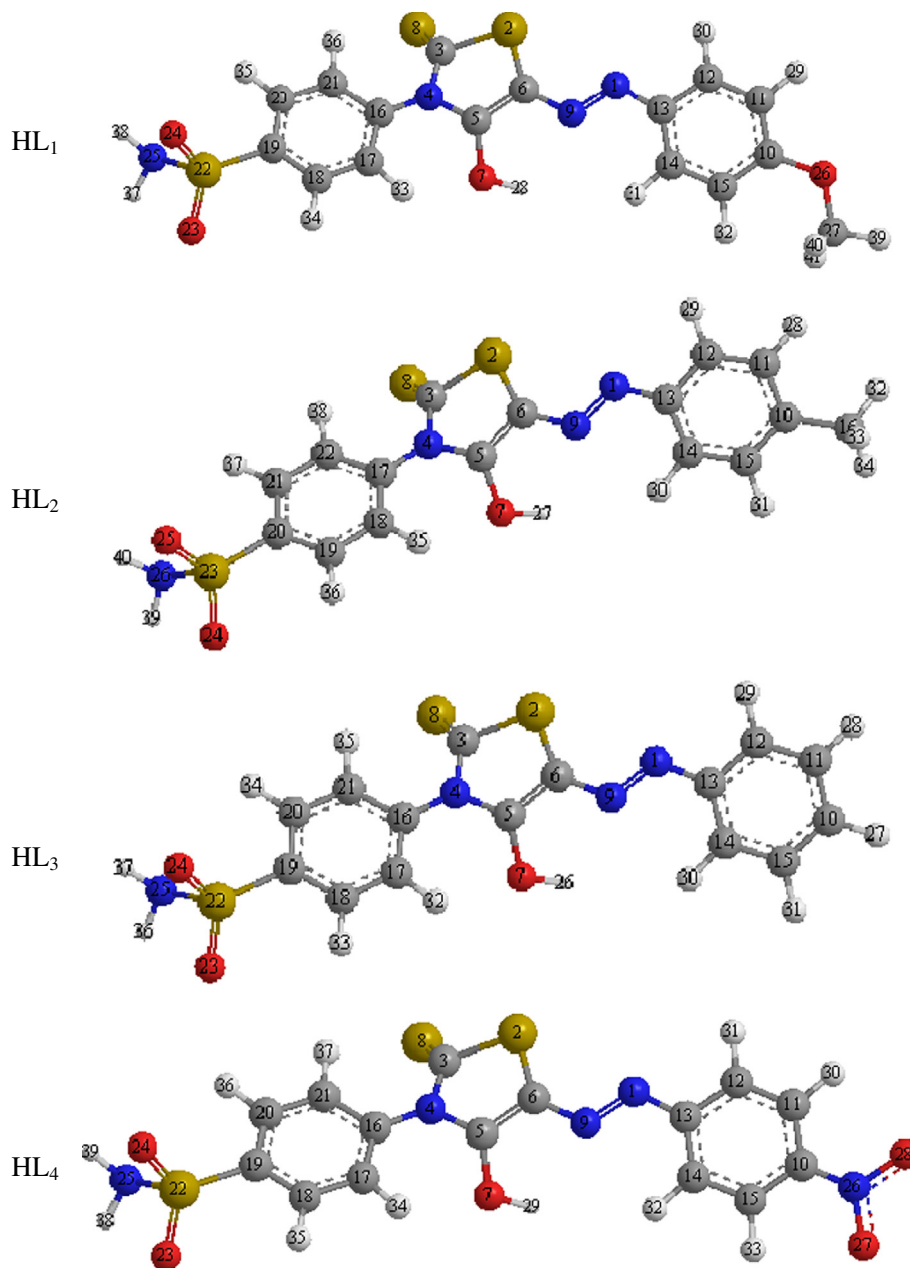


Fig. 4. The calculated molecular structures of the ligands ( $HL_n$ ).

### 3. Results and discussion

The results of physical properties of the prepared ligands ( $HL_n$ ) and their Ru(III) complexes (**1–4**) along with their elemental analysis are collected in Table 1. The analytical data of Ru(III) complexes indicated that the complexes have 1:2 (metal:ligand) stoichiometry. The Ru(III) complexes are stable in air and soluble in most common organic solvents. The molar conductance values for the ruthenium(III) complexes ( $10^{-3}$  M) are measured in DMF and these values are ( $50\text{--}75 \Omega^{-1} \text{cm}^2 \text{mol}^{-1}$ ) range indicating the electrolytic nature of the complexes (presence of  $\text{Cl}^-$  ion) [10,28]. The room temperature magnetic moment values ( $\mu_{\text{eff}}$ ) per ruthenium ion for the complexes were in 1.69–2.10 BM range. These values lie within the range of the spin only value of one unpaired electron [29], which corresponds to  $\text{Ru}^{3+}$  state (low spin).

As shown in Table 1, the values of yield (%) and/or melting point are related to the nature of the *p*-substituent as they increase according to

the following order  $p\text{-(NO}_2 > \text{H} > \text{CH}_3 > \text{OCH}_3)$ . This can be attributed to the fact that the effective charge increased due to the electron withdrawing *p*-substituent ( $HL_4$ ) while it decreased by the electrons donating character of ( $HL_1$  and  $HL_2$ ). This is in accordance with that expected from Hammett's constant ( $\sigma^R$ ) as shown in Fig. 3, correlate the yield (%) values with  $\sigma^R$  it is clear that all these values increase with increasing  $\sigma^R$ .

#### 3.1. IR spectra

The FTIR spectra provide valuable information regarding the nature of the functional group attached to the metal atom. By comparing the IR spectra of ligands with those of their Ru(III) complexes, the following features can be pointed out:

(1) The broad and strong intensity band due to  $\nu(\text{OH})$  group which appears in the  $3344\text{--}3350 \text{ cm}^{-1}$  region arises from the strong intra and intermolecular hydrogen bonding (Fig. 1C) of the free ligands [2].

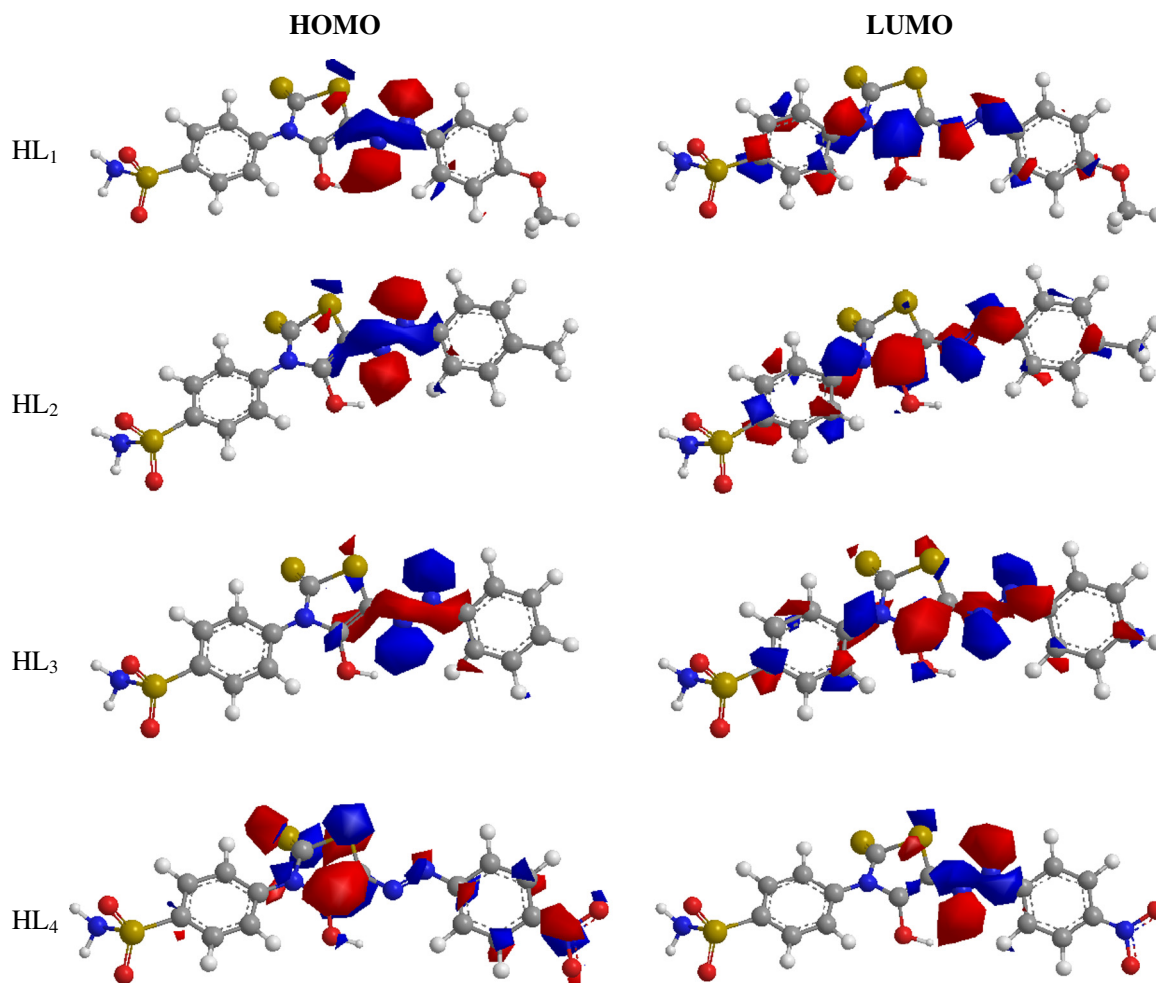


Fig. 5. The highest occupied molecular orbital (HOMO) and the lowest unoccupied molecular orbital (LUMO) of compounds (HL<sub>n</sub>).

(2) The two bands corresponding to  $\nu_{as}(\text{NH}_2)$  and  $\nu_s(\text{NH}_2)$  of the sulfonamide and  $\nu(\text{C}=\text{S})$  of the rhodanine moiety which appeared in the spectra of the ligands at 3253–3259, 2970–2978 and 908–914  $\text{cm}^{-1}$  regions, respectively, appeared almost at the same position in the spectra of their Ru(III) complexes [2], which can be taken as evidence that  $-\text{NH}_2$  and  $\text{C}=\text{S}$  groups are not taking part in the coordination to the Ru center.

(3) The bands due to  $\nu(\text{N}=\text{N})$  group which appeared in the spectra of the ligands at 1552–1558  $\text{cm}^{-1}$  region were shifted to lower wavenumbers by 13–17  $\text{cm}^{-1}$  indicating their coordination to the Ru center [3,11]. In the spectra of the ligands, the peak of the region 1693–1697  $\text{cm}^{-1}$  could be assigned to  $\text{C}=\text{C}$  stretching vibration and the absorbance at 1552–1556  $\text{cm}^{-1}$  region was ascribed to  $\text{C}=\text{N}$  stretching vibration of the synthesized ligands.

(4) Furthermore, the medium band corresponding to  $\nu(\text{C}-\text{O})$  of the rhodanine moiety which appeared in the spectra of the ligands at 1225–1242  $\text{cm}^{-1}$  disappears for all the complexes indicating that, the ligands coordinate through their deprotonated form and formation of metal–oxygen bonds [2,11]. This can be taken as an indication for the complete removal of hydrogen of OH group by the Ru(III) ion reacting with the ligands.

(5) The two bands corresponding to  $\nu_{as}(\text{SO}_2)$  and  $\nu_s(\text{SO}_2)$  of the sulfonamide moiety which appeared in the spectra of the ligands at 1326–1336 and 1225–1242  $\text{cm}^{-1}$  regions, respectively, appeared almost at the same position in the spectra of their Ru(III) complexes

[1], which can be taken as evidence that  $-\text{SO}_2$  group not taking part in the coordination to the Ru center.

(6) In addition, new bands were observed in the regions 600–634 and 538–551  $\text{cm}^{-1}$  which were assigned to the formation of Ru–O and Ru–N bonds, respectively [30]. This further supports the coordination of the oxygen atom of the deprotonated  $-\text{OH}$  of the rhodanine moiety (Fig. 1A) and nitrogen atom of the azo group ( $-\text{N}=\text{N}-$ ).

(6) The bands at 3050–3100 and 3850–2910  $\text{cm}^{-1}$  regions are assigned to  $\nu(\text{C}-\text{H})$  vibrations of the aromatic system in the spectra of the ligands and their complexes, respectively [31–33].

Intramolecular hydrogen bonds in the ligands involving OH group with the  $-\text{N}=\text{N}-$  group increased their stabilities through ring structure (Fig. 1C) [34–36]. The strength of the hydrogen bond of compounds depends on the nature of substituents present in the coupling component from the arylazo group.

### 3.2. Electronic spectra

The electronic spectra of all complexes (1–4) were recorded in dimethylformamide solvent in the range of 300–700 nm. The ground state of ruthenium(III) ion ( $t_{2g}^5$ -configuration) is  ${}^2T_{1g}$  and the first excited doublet levels, in order of increasing energy, are  ${}^2A_{2g}$  and  ${}^2T_{1g}$  arising from  $t_{2g}^4 e_g^1$  configuration. Bands that were observed in 586–605 nm region have been assigned to d–d transitions, while bands in the

488–515 nm region have been assigned to charge transfer transitions. These features indicate a low-spin octahedral geometry around Ru(III) ion [37].

### 3.3. $^1\text{H}$ NMR spectra

The  $^1\text{H}$  NMR spectra of all the ligands ( $\text{HL}_n$ ) were recorded in  $\text{DMSO-d}_6$  at room temperature. In the aromatic region, a few doublets and in few cases some overlapping doublets/multiplets are observed in the range of  $\delta \sim 7.60\text{--}8.00$  ppm due to the protons of benzene ring. Another singlet corresponding to one proton for all compounds is observed in the range of  $\delta \sim 10.60\text{--}11.70$  ppm. This signal disappeared when a  $\text{D}_2\text{O}$  exchange experiment was carried out. It can be assigned either to OH or NH, in either case it is strongly deshielded because of hydrogen bonding with the other atom (N/O). It may be noted that the integration of this signal perfectly matches with one proton and there is no other fragment(s) of this signal, which suggests that only one tautomeric form of the ligand exists in solution under the experimental conditions. Comparing with the solid state study, we prefer to assign this signal to

OH, however, assignment of this peak to NH cannot be ruled out provided that solid state structural evidence is not considered [29]. As reported in a previous study [1,2], this hydrogen bonding leads to a large deshielding of these protons. The signal due to  $\text{NH}_2$  protons appeared as singlet in the range of 7.10–7.42 ppm. The  $^1\text{H}$  NMR spectral data that are reported along with the possible assignments were found as to be in their expected region [3,4].

### 3.4. Molecular structure

The calculated molecular structures for ligands ( $\text{HL}_n$ ) are shown in Fig. 4. Primary calculations reveal that the azo form (B) is more stable and reactive than azo form (A) (Fig. 1). Molecular structures (HOMO & LUMO) are presented in Fig. 5 for ligands ( $\text{HL}_n$ ) [azo form (B)]. Selected geometric parameter bond lengths and bond angles are tabulated in Tables 2–5 for ligands ( $\text{HL}_n$ ) [azo form (B)]. The HOMO–LUMO energy gap ( $\Delta E$ ) is an important stability index which is applied to develop theoretical models for explaining the structure and conformation barriers in many molecular systems. The smaller is the value of  $\Delta E$ , the

**Table 2**  
The bond lengths and bond angles of  $\text{HL}_1$ .

Bond lengths (Å)		Bond angles (°)		Bond angles (°)	
C(27)–H(41)	1.113	H(41)–C(27)–H(40)	111.884	S(2)–C(3)–N(4)	107.825
C(27)–H(40)	1.113	H(41)–C(27)–H(39)	108.162	S(2)–C(3)–S(8)	118.62
C(27)–H(39)	1.113	H(41)–C(27)–O(26)	110.357	N(4)–C(3)–S(8)	128.715
N(25)–H(38)	1.019	H(40)–C(27)–H(39)	108.172	H(28)–O(7)–C(5)	110.869
N(25)–H(37)	1.019	H(40)–C(27)–O(26)	110.35	C(5)–N(4)–C(3)	106.002
C(21)–H(36)	1.1	H(39)–C(27)–O(26)	107.776	C(5)–N(4)–C(16)	127.888
C(20)–H(35)	1.104	H(38)–N(25)–H(37)	105.76	C(3)–N(4)–C(16)	126.09
C(18)–H(34)	1.104	H(38)–N(25)–S(22)	110.214	C(3)–S(2)–C(6)	88.432
C(17)–H(33)	1.098	H(37)–N(25)–S(22)	110.215	C(6)–C(5)–N(4)	117.385
C(15)–H(32)	1.102	N(25)–S(22)–O(24)	88.368	C(6)–C(5)–O(7)	118.011
C(14)–H(31)	1.103	N(25)–S(22)–O(23)	88.187	N(4)–C(5)–O(7)	122.276
C(12)–H(30)	1.104	N(25)–S(22)–C(19)	115.159	C(14)–C(13)–C(12)	116.861
C(11)–H(29)	1.104	O(24)–S(22)–O(23)	121.845	C(14)–C(13)–N(1)	126.058
O(7)–H(28)	0.971	O(24)–S(22)–C(19)	116.691	C(12)–C(13)–N(1)	117.081
C(16)–C(21)	1.353	O(23)–S(22)–C(19)	117.031	S(2)–C(6)–C(5)	110.655
C(20)–C(21)	1.343	H(35)–C(20)–C(21)	119.524	S(2)–C(6)–N(9)	131.135
C(19)–C(20)	1.339	H(35)–C(20)–C(19)	119.976	C(5)–C(6)–N(9)	118.195
C(18)–C(19)	1.339	C(21)–C(20)–C(19)	120.492	C(6)–N(9)–N(1)	119.486
C(17)–C(18)	1.343	C(20)–C(19)–C(18)	117.637	C(13)–N(1)–N(9)	119.468
C(16)–C(17)	1.352	C(20)–C(19)–S(22)	121.176		
C(10)–C(15)	1.348	C(18)–C(19)–S(22)	121.171		
C(14)–C(15)	1.343	H(34)–C(18)–C(19)	119.859		
C(13)–C(14)	1.346	H(34)–C(18)–C(17)	119.515		
C(12)–C(13)	1.345	C(19)–C(18)–C(17)	120.617		
C(11)–C(12)	1.341	H(36)–C(21)–C(16)	122.516		
C(10)–C(11)	1.347	H(36)–C(21)–C(20)	113.552		
C(3)–S(2)	1.788	C(16)–C(21)–C(20)	123.917		
C(6)–S(2)	1.481	H(33)–C(17)–C(18)	113.174		
C(5)–C(6)	1.36	H(33)–C(17)–C(16)	123.022		
N(4)–C(5)	1.29	C(18)–C(17)–C(16)	123.797		
C(3)–N(4)	1.276	C(10)–O(26)–C(27)	118.782		
S(22)–N(25)	1.701	H(32)–C(15)–C(10)	120.733		
S(22)–O(24)	1.466	H(32)–C(15)–C(14)	116.917		
S(22)–O(23)	1.466	C(10)–C(15)–C(14)	122.349		
C(19)–S(22)	1.786	C(15)–C(10)–C(11)	115.599		
N(4)–C(16)	1.288	C(15)–C(10)–O(26)	125.602		
C(13)–N(1)	1.268	C(11)–C(10)–O(26)	118.798		
C(10)–O(26)	1.375	H(29)–C(11)–C(12)	118.69		
C(6)–N(9)	1.269	H(29)–C(11)–C(10)	118.683		
N(1)–N(9)	1.252	C(12)–C(11)–C(10)	122.627		
C(3)–S(8)	1.58	H(31)–C(14)–C(15)	117.125		
C(5)–O(7)	1.368	H(31)–C(14)–C(13)	121.534		
O(26)–C(27)	1.409	C(15)–C(14)–C(13)	121.341		
		H(30)–C(12)–C(13)	120.335		
		H(30)–C(12)–C(11)	118.443		
		C(13)–C(12)–C(11)	121.222		
		C(21)–C(16)–C(17)	113.456		
		C(21)–C(16)–N(4)	122.44		
		C(17)–C(16)–N(4)	124.025		

**Table 3**  
The bond lengths and bond angles of HL<sub>2</sub>.

Bond lengths (Å)		Bond angles (°)		Bond angles (°)	
N(26)–H(40)	1.019	H(40)–N(26)–H(39)	105.758	S(2)–C(3)–S(8)	118.626
N(26)–H(39)	1.019	H(40)–N(26)–S(23)	110.222	N(4)–C(3)–S(8)	128.731
C(22)–H(38)	1.1	H(39)–N(26)–S(23)	110.215	H(27)–O(7)–C(5)	110.887
C(21)–H(37)	1.104	N(26)–S(23)–O(25)	88.401	C(5)–N(4)–C(3)	106.001
C(19)–H(36)	1.104	N(26)–S(23)–O(24)	88.196	C(5)–N(4)–C(17)	127.872
C(18)–H(35)	1.098	N(26)–S(23)–C(20)	115.093	C(3)–N(4)–C(17)	126.108
C(16)–H(34)	1.114	O(25)–S(23)–O(24)	121.822	C(3)–S(2)–C(6)	88.436
C(16)–H(33)	1.114	O(25)–S(23)–C(20)	116.691	C(6)–C(5)–N(4)	117.39
C(16)–H(32)	1.113	O(24)–S(23)–C(20)	117.06	C(6)–C(5)–O(7)	118.01
C(15)–H(31)	1.103	H(37)–C(21)–C(22)	119.52	N(4)–C(5)–O(7)	122.267
C(14)–H(30)	1.103	H(37)–C(21)–C(20)	119.975	C(14)–C(13)–C(12)	117.453
C(12)–H(29)	1.105	C(22)–C(21)–C(20)	120.498	C(14)–C(13)–N(1)	125.753
C(11)–H(28)	1.103	C(21)–C(20)–C(19)	117.633	C(12)–C(13)–N(1)	116.794
O(7)–H(27)	0.971	C(21)–C(20)–S(23)	121.174	S(2)–C(6)–C(5)	110.65
C(17)–C(22)	1.353	C(19)–C(20)–S(23)	121.178	S(2)–C(6)–N(9)	131.161
C(21)–C(22)	1.343	H(36)–C(19)–C(20)	119.867	C(5)–C(6)–N(9)	118.175
C(20)–C(21)	1.339	H(36)–C(19)–C(18)	119.508	C(6)–N(9)–N(1)	119.503
C(19)–C(20)	1.339	C(20)–C(19)–C(18)	120.616	C(13)–N(1)–N(9)	119.504
C(18)–C(19)	1.343	H(38)–C(22)–C(17)	122.517		
C(17)–C(18)	1.352	H(38)–C(22)–C(21)	113.554		
C(10)–C(15)	1.344	C(17)–C(22)–C(21)	123.914		
C(14)–C(15)	1.343	H(35)–C(18)–C(19)	113.172		
C(13)–C(14)	1.348	H(35)–C(18)–C(17)	123.017		
C(12)–C(13)	1.347	C(19)–C(18)–C(17)	123.804		
C(11)–C(12)	1.342	H(34)–C(16)–H(33)	108.464		
C(10)–C(11)	1.343	H(34)–C(16)–H(32)	107.225		
C(3)–S(2)	1.788	H(34)–C(16)–C(10)	110.63		
C(6)–S(2)	1.481	H(33)–C(16)–H(32)	107.775		
C(5)–C(6)	1.36	H(33)–C(16)–C(10)	110.032		
N(4)–C(5)	1.29	H(32)–C(16)–C(10)	112.567		
C(3)–N(4)	1.276	H(31)–C(15)–C(10)	119.33		
S(23)–N(26)	1.701	H(31)–C(15)–C(14)	119.412		
S(23)–O(25)	1.466	C(10)–C(15)–C(14)	121.258		
S(23)–O(24)	1.466	C(15)–C(10)–C(11)	117.935		
C(20)–S(23)	1.786	C(15)–C(10)–C(16)	120.418		
N(4)–C(17)	1.288	C(11)–C(10)–C(16)	121.646		
C(13)–N(1)	1.268	H(28)–C(11)–C(12)	119.203		
C(10)–C(16)	1.51	H(28)–C(11)–C(10)	119.963		
C(6)–N(9)	1.269	C(12)–C(11)–C(10)	120.834		
N(1)–N(9)	1.252	H(30)–C(14)–C(15)	117.054		
C(3)–S(8)	1.58	H(30)–C(14)–C(13)	121.918		
C(5)–O(7)	1.368	C(15)–C(14)–C(13)	121.028		
		H(29)–C(12)–C(13)	120.269		
		H(29)–C(12)–C(11)	118.239		
		C(13)–C(12)–C(11)	121.492		
		C(22)–C(17)–C(18)	113.452		
		C(22)–C(17)–N(4)	122.453		
		C(18)–C(17)–N(4)	124.015		
		S(2)–C(3)–N(4)	107.821		

more is the reactivity of the compound has [1,2]. The calculated quantum chemical parameters are given in Table 6. Additional parameters such as separation energies,  $\Delta E$ , absolute electronegativities,  $\chi$ , chemical potentials,  $Pi$ , absolute hardness,  $\eta$ , absolute softness,  $\sigma$ , global electrophilicity,  $\omega$ , global softness,  $S$  and additional electronic charge, and  $\Delta N_{\max}$ , have been calculated according to the following Eqs. (2–9) [3,38]:

$$\Delta E = E_{LUMO} - E_{HOMO} \quad (2)$$

$$\chi = \frac{-(E_{HOMO} + E_{LUMO})}{2} \quad (3)$$

$$\eta = \frac{E_{LUMO} - E_{HOMO}}{2} \quad (4)$$

$$\sigma = 1/\eta \quad (5)$$

$$Pi = -\chi \quad (6)$$

$$S = \frac{1}{2\eta} \quad (7)$$

$$\omega = Pi^2/2\eta \quad (8)$$

$$\Delta N_{\max} = -Pi/\eta. \quad (9)$$

### 3.5. Thermal analyses

The thermal properties of ligands (HL<sub>2</sub>, HL<sub>3</sub> and HL<sub>4</sub>) and their Ru(III) complexes (**2**, **3** and **4**) were characterized on the basis of thermogravimetric analysis (TGA). The temperature intervals and the percentage of loss of masses of the ligands are listed in Table 7. It is clear that the change of substituent affects the thermal properties of the ligands (Fig. 6).

HL<sub>2</sub> ligand shows four decomposition steps, the first stage occurs in the temperature range of 50–200 °C is attributed to loss of C<sub>6</sub>H<sub>7</sub> (Found 19.01% and calc. 19.43%). The second stage in the temperature range of

**Table 4**  
The bond lengths and bond angles of HL<sub>3</sub>.

Bond lengths (Å)		Bond angles (°)		Bond angles (°)	
N(25)–H(37)	1.019	H(37)–N(25)–H(36)	105.757	C(3)–S(2)–C(6)	88.428
N(25)–H(36)	1.019	H(37)–N(25)–S(22)	110.226	C(6)–C(5)–N(4)	117.383
C(21)–H(35)	1.1	H(36)–N(25)–S(22)	110.213	C(6)–C(5)–O(7)	118.021
C(20)–H(34)	1.104	N(25)–S(22)–O(24)	88.386	N(4)–C(5)–O(7)	122.269
C(18)–H(33)	1.104	N(25)–S(22)–O(23)	88.218	C(14)–C(13)–C(12)	117.769
C(17)–H(32)	1.098	N(25)–S(22)–C(19)	115.068	C(14)–C(13)–N(1)	125.638
C(15)–H(31)	1.103	O(24)–S(22)–O(23)	121.82	C(12)–C(13)–N(1)	116.593
C(14)–H(30)	1.103	O(24)–S(22)–C(19)	116.691	S(2)–C(6)–C(5)	110.647
C(12)–H(29)	1.105	O(23)–S(22)–C(19)	117.069	S(2)–C(6)–N(9)	131.121
C(11)–H(28)	1.103	H(34)–C(20)–C(21)	119.519	C(5)–C(6)–N(9)	118.217
C(10)–H(27)	1.103	H(34)–C(20)–C(19)	119.98	C(6)–N(9)–N(1)	119.465
O(7)–H(26)	0.971	C(21)–C(20)–C(19)	120.494	C(13)–N(1)–N(9)	119.59
C(16)–C(21)	1.353	C(20)–C(19)–C(18)	117.635		
C(20)–C(21)	1.343	C(20)–C(19)–S(22)	121.151		
C(19)–C(20)	1.339	C(18)–C(19)–S(22)	121.199		
C(18)–C(19)	1.339	H(33)–C(18)–C(19)	119.864		
C(17)–C(18)	1.343	H(33)–C(18)–C(17)	119.509		
C(16)–C(17)	1.352	C(19)–C(18)–C(17)	120.618		
C(10)–C(15)	1.341	H(35)–C(21)–C(16)	122.518		
C(14)–C(15)	1.343	H(35)–C(21)–C(20)	113.55		
C(13)–C(14)	1.348	C(16)–C(21)–C(20)	123.918		
C(12)–C(13)	1.348	H(32)–C(17)–C(18)	113.179		
C(11)–C(12)	1.342	H(32)–C(17)–C(16)	123.016		
C(10)–C(11)	1.341	C(18)–C(17)–C(16)	123.798		
C(3)–S(2)	1.788	H(31)–C(15)–C(10)	119.645		
C(6)–S(2)	1.481	H(31)–C(15)–C(14)	120.033		
C(5)–C(6)	1.36	C(10)–C(15)–C(14)	120.322		
N(4)–C(5)	1.29	H(27)–C(10)–C(15)	120.311		
C(3)–N(4)	1.276	H(27)–C(10)–C(11)	120.289		
S(22)–N(25)	1.701	C(15)–C(10)–C(11)	119.399		
S(22)–O(24)	1.466	H(28)–C(11)–C(12)	120.117		
S(22)–O(23)	1.466	H(28)–C(11)–C(10)	119.895		
C(19)–S(22)	1.786	C(12)–C(11)–C(10)	119.988		
N(4)–C(16)	1.288	H(30)–C(14)–C(15)	116.99		
C(13)–N(1)	1.268	H(30)–C(14)–C(13)	121.944		
C(6)–N(9)	1.269	C(15)–C(14)–C(13)	121.066		
N(1)–N(9)	1.252	H(29)–C(12)–C(13)	120.367		
C(3)–S(8)	1.581	H(29)–C(12)–C(11)	118.178		
C(5)–O(7)	1.368	C(13)–C(12)–C(11)	121.455		
		C(21)–C(16)–C(17)	113.454		
		C(21)–C(16)–N(4)	122.433		
		C(17)–C(16)–N(4)	124.034		
		S(2)–C(3)–N(4)	107.818		
		S(2)–C(3)–S(8)	118.617		
		N(4)–C(3)–S(8)	128.725		
		H(26)–O(7)–C(5)	110.884		
		C(5)–N(4)–C(3)	106		
		C(5)–N(4)–C(16)	127.896		
		C(3)–N(4)–C(16)	126.085		

200–300 °C corresponding to loss of a part of the ligand (C<sub>6</sub>H<sub>6</sub>N<sub>2</sub> SO<sub>2</sub>) (Found 38.58%, calc. 38.87%). The third stage in the temperature range of 300–600 °C corresponding to loss of a part of the ligand (SO<sub>2</sub>NH<sub>2</sub>) (Found 19.23%, calc. 19.68%). The fourth stage in the temperature ranges >600 °C corresponding to loss of carbon atoms (Found 22.1%, calc. 22.00%).

HL<sub>3</sub> ligand shows loss of (Found 19.95%, calc. 19.62%) in the temperature range of 50–200 °C corresponding to loss of C<sub>6</sub>H<sub>5</sub> while the weight loss in the temperature range of 200–300 °C (Found 43.02%, calc. 43.31%), which is attributed to loss of a part of the ligand (C<sub>6</sub>H<sub>6</sub>N<sub>2</sub> SO<sub>2</sub>) and at 300–600 °C corresponding to loss of (SO<sub>2</sub>NH<sub>2</sub>) (Found 21.00%, calc. 20.38%). Finally, the residue is carbon atoms.

TG curve of the HL<sub>4</sub> ligand shows two steps of decomposition. The first stage of decomposition occurs in the temperature range of 50–200 °C and is associated with the loss of a part of the ligand (NO<sub>2</sub>) with an estimated weight loss of 10.27% (calcd. 10.51%). The second stage of decomposition occurs in the temperature range of 200–300 °C and is associated with the loss of C<sub>12</sub>H<sub>11</sub>N<sub>3</sub>SO<sub>3</sub> molecule and with an estimated weight loss of 70.03% (calcd. 70.63%). The

third stage of decomposition occurs in the temperature range of 300–600 °C and is associated with the loss of nitrogen and sulfur molecules and with an estimated weight loss of 11.00% (calcd. 10.51%). There after the weight of the residue corresponds to carbon atoms.

All Ru(III) complexes (2, 3 and 4) showed TG curves in the temperature range of ~100–220 °C loss of bipy + 1/2 Cl<sub>2</sub> molecules. The second stage is related to loss of the part of ligand. The final weight losses are due to the decomposition of the rest of the ligand and metal oxide residue (Table 8).

### 3.6. Calculation of activation thermodynamic parameters

The thermodynamic activation parameters of decomposition processes of the ligands (HL<sub>2</sub>, HL<sub>3</sub> and HL<sub>4</sub>) and their Ru(III) complexes (2, 3 and 4) namely activation energy (*E<sub>a</sub>*), enthalpy ( $\Delta H^*$ ), entropy ( $\Delta S^*$ ), and Gibbs free energy change of the decomposition ( $\Delta G^*$ ) are evaluated graphically by employing the Coats–Redfern [39] and Horowitz–Metzger [40] methods.

**Table 5**  
The bond lengths and bond angles of HL<sub>4</sub>.

Bond lengths (Å)		Bond angles (°)		Bond angles (°)	
N(25)–H(39)	1.019	H(39)–N(25)–H(38)	105.738	H(29)–O(7)–C(5)	111.178
N(25)–H(38)	1.019	H(39)–N(25)–S(22)	110.197	C(5)–N(4)–C(3)	105.793
C(21)–H(37)	1.099	H(38)–N(25)–S(22)	110.202	C(5)–N(4)–C(16)	127.859
C(20)–H(36)	1.104	N(25)–S(22)–O(24)	88.311	C(3)–N(4)–C(16)	126.326
C(18)–H(35)	1.104	N(25)–S(22)–O(23)	88.136	C(3)–S(2)–C(6)	88.408
C(17)–H(34)	1.098	N(25)–S(22)–C(19)	115.26	C(6)–C(5)–N(4)	117.516
C(15)–H(33)	1.104	O(24)–S(22)–O(23)	121.832	C(6)–C(5)–O(7)	117.996
C(14)–H(32)	1.103	O(24)–S(22)–C(19)	116.625	N(4)–C(5)–O(7)	122.149
C(12)–H(31)	1.105	O(23)–S(22)–C(19)	117.112	C(14)–C(13)–C(12)	117.12
C(11)–H(30)	1.104	H(36)–C(20)–C(21)	119.514	C(14)–C(13)–N(1)	125.219
O(7)–H(29)	0.971	H(36)–C(20)–C(19)	119.986	C(12)–C(13)–N(1)	117.661
C(16)–C(21)	1.353	C(21)–C(20)–C(19)	120.492	S(2)–C(6)–C(5)	110.624
C(20)–C(21)	1.343	C(20)–C(19)–C(18)	117.628	S(2)–C(6)–N(9)	131.176
C(19)–C(20)	1.339	C(20)–C(19)–S(22)	121.173	C(5)–C(6)–N(9)	118.181
C(18)–C(19)	1.339	C(18)–C(19)–S(22)	121.179	C(6)–N(9)–N(1)	119.433
C(17)–C(18)	1.343	H(35)–C(18)–C(19)	119.852	C(13)–N(1)–N(9)	119.109
C(16)–C(17)	1.352	H(35)–C(18)–C(17)	119.525		
C(10)–C(15)	1.347	C(19)–C(18)–C(17)	120.614		
C(14)–C(15)	1.342	H(37)–C(21)–C(16)	122.552		
C(13)–C(14)	1.347	H(37)–C(21)–C(20)	113.484		
C(12)–C(13)	1.345	C(16)–C(21)–C(20)	123.948		
C(11)–C(12)	1.343	H(34)–C(17)–C(18)	113.136		
C(10)–C(11)	1.347	H(34)–C(17)–C(16)	123.03		
C(3)–S(2)	1.788	C(18)–C(17)–C(16)	123.826		
C(6)–S(2)	1.481	C(10)–N(26)–O(28)	122.771		
C(5)–C(6)	1.361	C(10)–N(26)–O(27)	123.008		
N(4)–C(5)	1.29	O(28)–N(26)–O(27)	114.221		
C(3)–N(4)	1.276	H(33)–C(15)–C(10)	121.178		
S(22)–N(25)	1.701	H(33)–C(15)–C(14)	117.147		
S(22)–O(24)	1.466	C(10)–C(15)–C(14)	121.675		
S(22)–O(23)	1.466	C(15)–C(10)–C(11)	116.841		
C(19)–S(22)	1.786	C(15)–C(10)–N(26)	121.24		
N(4)–C(16)	1.289	C(11)–C(10)–N(26)	121.919		
C(13)–N(1)	1.268	H(30)–C(11)–C(12)	117.231		
C(10)–N(26)	1.257	H(30)–C(11)–C(10)	121.202		
C(6)–N(9)	1.269	C(12)–C(11)–C(10)	121.567		
N(1)–N(9)	1.252	H(32)–C(14)–C(15)	116.735		
C(3)–S(8)	1.58	H(32)–C(14)–C(13)	121.915		
C(5)–O(7)	1.368	C(15)–C(14)–C(13)	121.35		
N(26)–O(28)	1.313	H(31)–C(12)–C(13)	120.015		
N(26)–O(27)	1.314	H(31)–C(12)–C(11)	118.539		
		C(13)–C(12)–C(11)	121.446		
		C(21)–C(16)–C(17)	113.409		
		C(21)–C(16)–N(4)	122.494		
		C(17)–C(16)–N(4)	124.014		
		S(2)–C(3)–N(4)	107.978		
		S(2)–C(3)–S(8)	118.851		
		N(4)–C(3)–S(8)	128.835		

### 3.6.1. Coats–Redfern equation

The Coats–Redfern equation, which is a typical integral method, can represent as:

$$\int_0^{\alpha} \frac{dx}{(1-\alpha)^n} = \frac{A}{\varphi} \int_1^2 \exp\left(-\frac{E_a}{RT}\right) dt. \quad (10)$$

For convenience of integration, the lower limit  $T_1$  is usually taken as zero. This equation on integration gives:

$$\ln\left[-\frac{\ln(1-\alpha)}{T^2}\right] = -\frac{E_a}{RT} + \ln\left[\frac{AR}{\varphi E_a}\right]. \quad (11)$$

**Table 6**  
The calculated quantum chemical properties for the ligands (HL<sub>n</sub>).

Compound	E <sub>HOMO</sub> (a.u.)	E <sub>LUMO</sub> (a.u.)	ΔE (a.u.)	χ (a.u.)	η (a.u.)	σ (a.u.) <sup>-1</sup>	Pi (a.u.)	S (a.u.) <sup>-1</sup>	ω (a.u.)	ΔN <sub>max</sub> (a.u.)
HL <sub>1</sub>										
(A)	-0.1235	-0.0895	0.0341	0.1065	0.0170	58.719	-0.1065	29.359	0.3329	6.253
(B)	-0.0840	-0.0698	0.0142	0.0769	0.0071	140.944	-0.0769	70.472	0.4169	10.841
HL <sub>2</sub>										
(A)	-0.1236	-0.1014	0.0222	0.1125	0.0111	90.131	-0.1125	45.065	0.5706	10.142
(B)	-0.0844	-0.0741	0.0103	0.0793	0.0052	194.364	-0.0793	97.182	0.6106	15.406
HL <sub>3</sub>										
(A)	-0.1239	-0.1089	0.0151	0.1164	0.0075	132.714	-0.1164	66.3572	0.8988	15.446
(B)	-0.0849	-0.0765	0.0084	0.0807	0.0042	238.664	-0.0807	119.332	0.7771	19.260
HL <sub>4</sub>										
(A)	-0.2145	-0.1219	0.0925	0.1682	0.0463	21.615	-0.1682	10.807	0.3059	3.637
(B)	-0.1353	-0.0839	0.0514	0.1096	0.0257	38.880	-0.1096	19.440	0.23369	4.262

**Table 7**  
Thermal analyses data for the ligands (HL<sub>n</sub>).

Compound	Temp. range (°C)	Calc. mass loss (found) %	Assignment
HL <sub>2</sub>	50–200	19.43 (19.01)	Loss of C <sub>6</sub> H <sub>7</sub>
	200–300	38.87 (38.58)	Loss of C <sub>6</sub> H <sub>6</sub> N <sub>2</sub> SO <sub>2</sub>
	300–600	19.68 (19.23)	Loss of SO <sub>2</sub> NH <sub>2</sub>
	>600	22.00 (22.10)	Loss of carbon atoms
HL <sub>3</sub>	50–200	19.62 (19.95)	Loss of C <sub>6</sub> H <sub>5</sub>
	200–300	43.31 (43.02)	Loss of C <sub>6</sub> H <sub>6</sub> N <sub>2</sub> SO <sub>2</sub>
	300–600	20.38 (21.00)	Loss of SO <sub>2</sub> NH <sub>2</sub>
	>600	16.67 (16.00)	Loss of carbon atoms
HL <sub>4</sub>	50–200	10.51 (10.27)	Loss of NO <sub>2</sub>
	200–300	70.63 (69.03)	Loss of
	300–600	10.51 (11.00)	C <sub>12</sub> H <sub>11</sub> N <sub>3</sub> O <sub>3</sub> S
	>600	8.35 (10.05)	Loss of nitrogen and sulfur Loss of carbon atoms

A plot of left-hand side (LHS) against 1/T was drawn (Fig. 7).  $E_a$  is the energy of activation in J mol<sup>-1</sup> and calculated from the slope and A in (s<sup>-1</sup>) from the intercept value. The entropy of activation ( $\Delta S^*$ ) in (J mol<sup>-1</sup> K<sup>-1</sup>) calculated by using the equation:

$$\Delta S^* = 2.303 \left[ \log \left( \frac{Ah}{k_B T_s} \right) \right] R \quad (12)$$

where  $k_B$  is the Boltzmann constant,  $h$  is the Plank's constant and  $T_s$  is the TG peak temperature.

### 3.6.2. Horowitz–Metzger equation

The Horowitz–Metzger equation is an illustrative of the approximation methods. These authors derived the relation:

$$\log \left[ \frac{1 - (1 - \alpha)^{1-n}}{1 - n} \right] = \frac{E_a \theta}{2.303 RT_s^2}, \text{ for } n \neq 1 \quad (13)$$

when  $n = 1$ , the LHS of Eq. (13) would be  $\log[-\log(1 - \alpha)]$  (Fig. 8). For a first order kinetic process, the Horowitz–Metzger equation may write in the form:

$$\log \left[ \log \left( \frac{W_\alpha}{W_\gamma} \right) \right] = \frac{E_a \theta}{2.303 RT_s^2} \log 2.303 \quad (14)$$

where  $\theta = T - T_s$ ,  $w_\gamma = w_\alpha - w$ ,  $w_\alpha$  = mass loss at the completion reaction;  $w$  = mass loss up to time  $t$ . The plot of  $\log[\log(w_\alpha/w_\gamma)]$  vs.  $\theta$

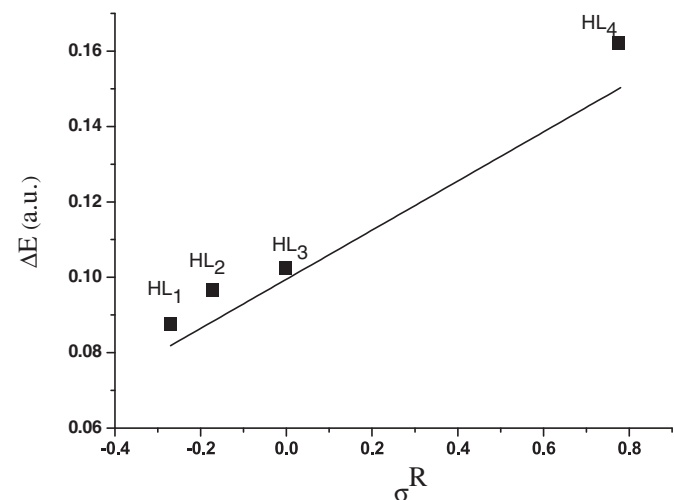


Fig. 6. The relation between Hammett's substitution coefficients ( $\sigma^R$ ) vs. energy gap ( $\Delta E$ ).

**Table 8**  
Thermal analyses data for Ru(III) complexes (2, 3 and 4).

Complex <sup>a</sup>	Temp. range (°C)	Found mass loss (calc.) %	Assignment
(2)	100–220	17.52 (17.50)	Loss of bipy + 1/2Cl <sub>2</sub>
	220–800	70.44 (70.50)	Loss of C <sub>32</sub> H <sub>26</sub> N <sub>12</sub> O <sub>4</sub> S <sub>6</sub>
	>800	12.04 (12.00)	RuO <sub>2</sub>
(3)	100–220	17.97 (18.03)	Loss of bipy + 1/2Cl <sub>2</sub>
	200–800	69.68 (70.00)	Loss of C <sub>30</sub> H <sub>20</sub> N <sub>12</sub> O <sub>4</sub> S <sub>6</sub>
(4)	>800	12.35 (12.05)	Loss of RuO <sub>2</sub>
	100–220	16.68 (16.50)	Loss of bipy + 1/2Cl <sub>2</sub>
	220–800	72.02 (72.00)	Loss of C <sub>30</sub> H <sub>20</sub> N <sub>14</sub> O <sub>8</sub> S <sub>6</sub>
	>800	11.39 (11.50)	Loss of RuO <sub>2</sub>

<sup>a</sup> Numbers as given in Table 1.

was drawn and found to be linear from the slope of which  $E_a$  was calculated. The pre-exponential factor, A, calculated from equation:

$$\frac{E_a}{RT_s^2} = \frac{A}{\left[ \varphi \exp \left( -\frac{E_a}{RT_s} \right) \right]} \quad (15)$$

The entropy of activation,  $\Delta S^*$ , is calculated from Eq. (12). The enthalpy activation,  $\Delta H^*$ , and Gibbs free energy,  $\Delta G^*$ , calculated from:

$$\Delta H^* = E_a - RT \quad (16)$$

$$\Delta G^* = \Delta H^* - T \Delta S^* \quad (17)$$

The calculated values of  $E_a$ , A,  $\Delta S^*$ ,  $\Delta H^*$  and  $\Delta G^*$  for the decomposition steps for ligands (HL<sub>2</sub>, HL<sub>3</sub> and HL<sub>4</sub>) and their Ru(III) complexes (2, 3 and 4) are summarized in Table 9.

### 3.7. DNA binding studies

Absorption titration is one of the most universally employed methods to study the binding modes and binding extent of compounds to DNA. Absorption titration experiments were performed with fixed concentrations of the ligands (HL<sub>1</sub>–HL<sub>4</sub>) (40 μM) while gradually increasing the concentration of DNA (10 mM) at 25 °C. While measuring the absorption spectra, an equal amount of DNA was added to both the compound solution and the reference solution to eliminate the absorbance of DNA itself. We have determined the intrinsic binding constant to CT-DNA by monitoring the absorption intensity of the charge transfer spectral bands near 298, 298, 299 and 293 nm for the ligands HL<sub>1</sub>, HL<sub>2</sub>, HL<sub>3</sub> and HL<sub>4</sub>, respectively. Upon the addition of increasing amount of CT-DNA, a significant “hyperchromic” effect was observed accompanied by a moderate red shift of 2–3 nm, indicative of stabilization of the DNA helix. These spectral characteristic suggests that the ligands bind either to the external contact (electrostatic binding) or to the major and minor grooves of DNA. Moreover, this “hyperchromic effect” can be explained on the basis of two phenomena. The large surface area of the ligand as well as the presence of planar aromatic chromophore facilitates a strong binding interaction of the ligands with CT-DNA. This groove binding results in structural reorganization of CT-DNA which entails partial unwinding or damage of the double helix at the exterior phosphate backbone leading to the formation of a cavity to accommodate the compound [41]. The intrinsic binding constants ( $K_b$ ) of all the ligands (HL<sub>1</sub>–HL<sub>4</sub>) with CT-DNA were determined (Eq. (1)) [42]. The  $K_b$  values obtained from the absorption spectral technique for ligands HL<sub>1</sub>, HL<sub>2</sub>, HL<sub>3</sub> and HL<sub>4</sub> were calculated as  $2.86 \times 10^4$ ,  $5.85 \times 10^4$ ,  $7.44 \times 10^4$  and  $2.32 \times 10^6$  M<sup>-1</sup>, respectively. The higher values of the binding constant of the ligands HL<sub>4</sub> are due to the presence of electron withdrawing group NO<sub>2</sub>.

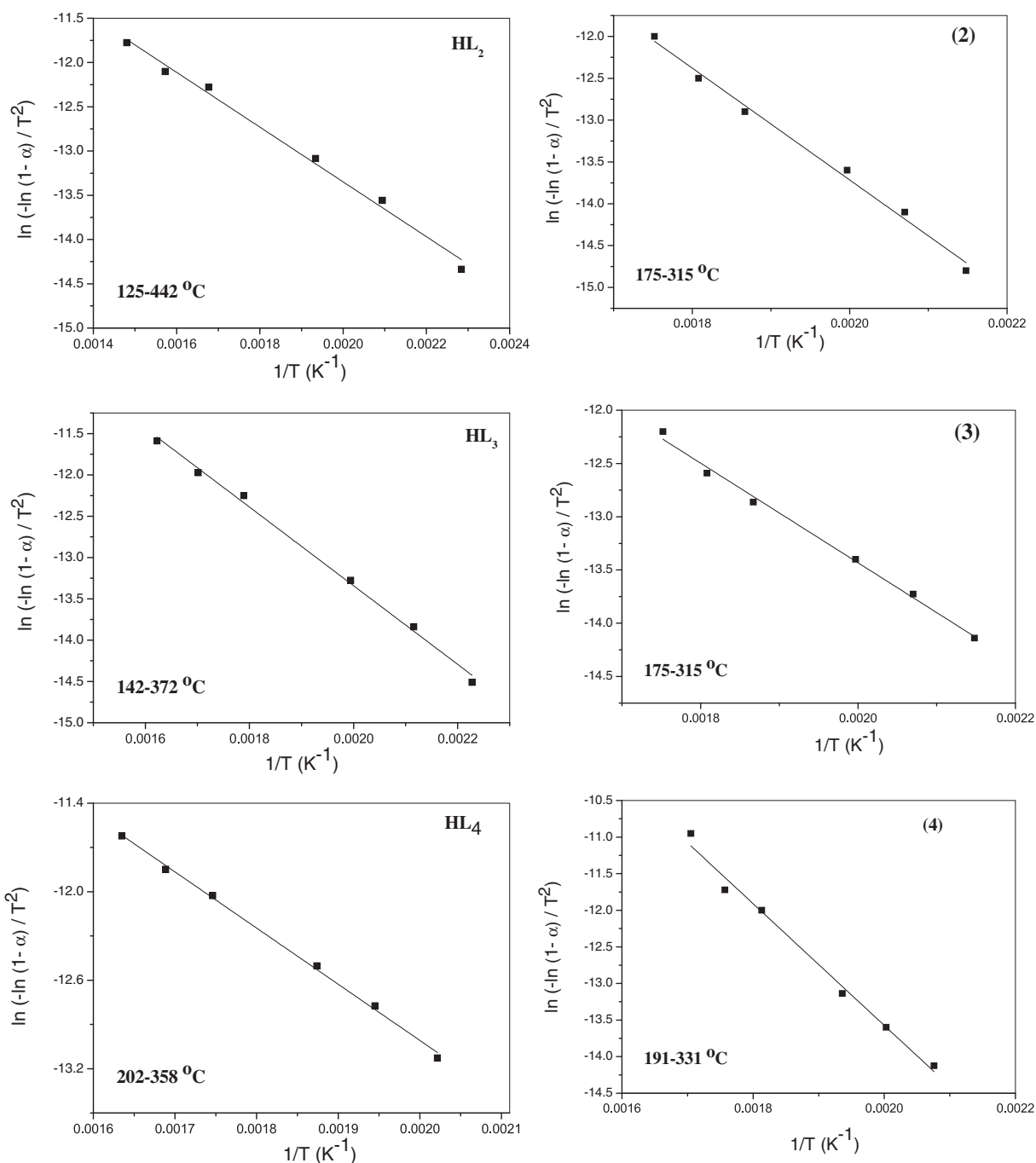


Fig. 7. Coats-Redfern (CR) of the ligands (HL<sub>2</sub>, HL<sub>3</sub> and HL<sub>4</sub>) and their Ru(III) complexes (2, 3 and 4).

### 3.8. Catalytic oxidation of benzylamine to benzonitrile

Many ruthenium(III) complexes [43,44] have been used as catalysts for dehydrogenation of benzylamine to benzonitrile with N-methylmorpholine-N-oxide (NMO). However, catalytic methods based on transition metals need stringent reaction conditions and high cost of the ligand, or have the disadvantages like long reaction time and high temperature. Therefore, the development of practical, inexpensive, simple and green chemical process for dehydrogenation is still needed. We are interested in the use of NMO, since it is soluble in organic solvents [23].

Herein, we present a simple protocol that adopts three fold excess of NMO as a co-oxidant and the prepared ruthenium(III) complexes as a

catalysts for dehydrogenation of benzylamine to benzonitrile in 65 to 80% yield. The catalytic dehydrogenation reactions were carried out at room temperature, in the presence of catalytic amount of the complexes,  $[Ru(L_n)_2(bipy)]Cl$  and an excess of NMO as a co-oxidant, according to the following: benzylamine (2 mmol) was added to the solution of the complex (5% mol in 5 cm<sup>3</sup> DMF) and NMO (3 mmol) was dissolved in 5 mL DMF. The reaction mixture was stirred at room temperature for 3 h, then benzonitrile was then isolated and weighed. The results for the catalytic dehydrogenation of benzylamine by the prepared complexes are summarized in Table 10. The yields and turnover frequency (TOF) are calculated.

A blank experiment was also carried out which revealed that in the absence of the complex, benzonitrile was not detected, suggesting that

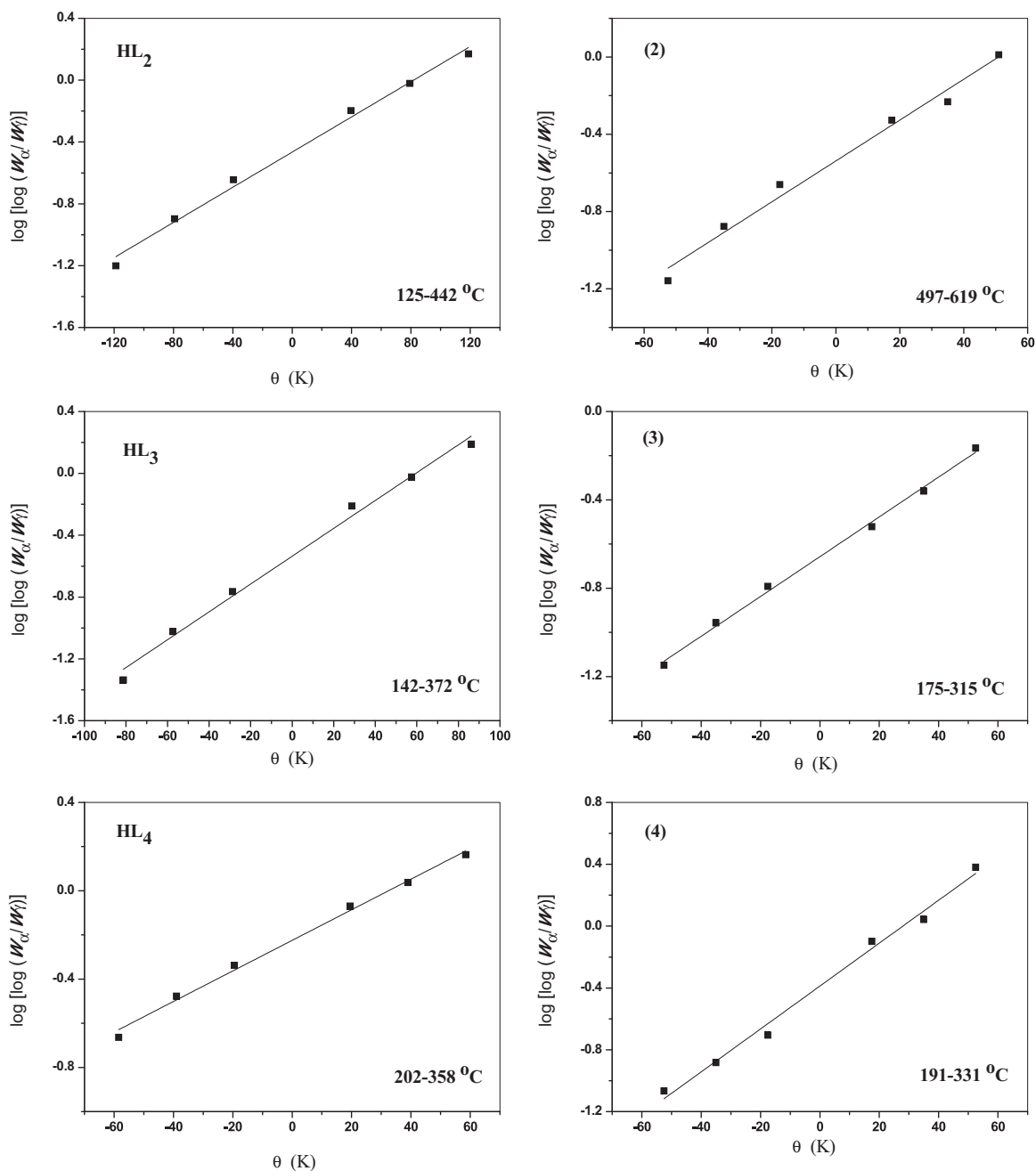


Fig. 8. Horowitz–Metzger (HM) of the ligands (HL<sub>2</sub>, HL<sub>3</sub> and HL<sub>4</sub>) and their Ru(III) complexes (**2**, **3** and **4**).

in the absence of the ruthenium complex, NMO itself is not able to dehydrogenate benzylamine, while in the presence of the ruthenium complex, NMO is able to trigger a recycling of the active species which expected to be ruthenium-oxo species ( $\text{Ru}^{\text{IV}} = \text{O}$ ). Recently, we reported the catalytic dehydrogenation of benzylamine to benzonitrile by  $[\text{Ru}^{\text{III}}\text{Cl}(\text{8-hq})_2\text{H}_2\text{O}]/\text{NMO}$  and suggested the formation of ruthenium-oxo species ( $\text{Ru}^{\text{IV}} = \text{O}$ ) [23]. However, upon comparing our catalyst system with other systems in the literature [27,45], it was found that the catalyst systems, Au/CeO<sub>2</sub>-direct anionic exchange/O<sub>2</sub> [43] and HNO<sub>3</sub>-promoted/nanotubes (CNTs/O<sub>2</sub>) [44] dehydrogenate benzylamine to benzonitrile in 89% and the reaction is 5 h.

It was noticed that our reaction times are shorter and yields of obtained benzonitrile by our catalysts systems are nearly comparable with those reported in the previously mentioned catalyst systems [46, 47] in addition reactions were carried out at room temperature. The catalytic oxidation of benzylamine under the same conditions has

been repeated in the presence of some other co-oxidants like NaIO<sub>4</sub>, K<sub>2</sub>S<sub>2</sub>O<sub>8</sub>, NaBrO<sub>3</sub> and NaOCl instead of H<sub>2</sub>O<sub>2</sub> and gave very low yield of benzonitrile (less than 5%). This is probably due to the formation of the solid precipitates NaIO<sub>3</sub>, K<sub>2</sub>SO<sub>4</sub>, NaBr and NaCl, which are all insoluble in DMF and remain at the end of the reaction and make the work up is difficult. We conclude that the use of NMO is preferred co-oxidant for oxidation of benzylamine in the presence of these complexes. In summary, these complexes catalytically oxidize benzylamine to benzonitrile in good yields at room temperature and in the presence of excess NMO as co-oxidant as well as this procedure is safe and simple for benzylamine.

#### 4. Conclusions

The structure of Ru(III) complexes of the ligands (HL<sub>n</sub>) were confirmed by elemental analyses, IR, <sup>1</sup>H NMR spectra, molar conductance

**Table 9**  
Kinetic parameters of the ligands (HL<sub>n</sub>) and their Ru(III) complexes (**2**, **3** and **4**).

Compound <sup>a</sup>	Decomposition temperature (°C)	Method	Parameters					Correlation coefficient ®
			$E_a$	$A$	$\Delta S^\ddagger$	$\Delta H^\ddagger$	$\Delta G^\ddagger$	
			(kJ mol <sup>-1</sup> )	(s <sup>-1</sup> )	(J mol <sup>-1</sup> K <sup>-1</sup> )	(kJ mol <sup>-1</sup> )	(kJ mol <sup>-1</sup> )	
HL <sub>2</sub>	125–442	CR	28.8	1.21	-249	24.0	168	0.9956
		HM	38.1	6.5	-235	33.3	169	0.9972
HL <sub>3</sub>	142–372	CR	25.7	0.4	-258	24.1	165	0.9911
		HM	33.8	3.21	-240	29.1	163	0.9916
HL <sub>4</sub>	202–358	CR	40	191	-225	35.6	155	0.9955
		HM	48.5	207	-205	44.1	153	0.9906
<b>2</b>	175–315	CR	55.8	788	-194	51.3	152	0.9912
		HM	65	175	-168	60.7	148	0.9932
<b>3</b>	175–315	CR	38.9	13.2	-228	34.6	153	0.9939
		HM	46.3	162	-207	42.0	149	0.9959
<b>4</b>	191–331	CR	69.1	$2.94 \times 10^4$	-164	64.7	152	0.9878
		HM	75.8	$1.39 \times 10^5$	-151	71.4	152	0.9881

<sup>a</sup> Numbers as given in Table 1.**Table 10**  
Catalytic oxidation of benzylamine by the prepared ruthenium(III) complexes.

Complex <sup>a</sup>	Yield	TOF, h <sup>-1</sup>
1	80	4.44
2	73	4.05
3	75	4.16
4	77	4.27

Reaction conditions: Reactions were carried out at room temperature: benzylamine (2 mmol), the complex (in 5 cm<sup>3</sup> DMF) and NMO (3 mmol), reaction time = 3 h. (TOF = turnover frequency = moles of product/moles of catalyst/time).

<sup>a</sup> Numbers as given in Table 1.

and thermal analysis data. Therefore, from IR spectrum, it is concluded that HL<sub>n</sub> binds to the Ru(III) as a monobasic bidentate ligand by coordinating *via* the nitrogen atom of the azo group (—N=N—) and oxygen atom of the deprotonated —OH group of the rhodanine moiety. The optimized bond lengths, bond angles and calculated quantum chemical parameters for the ligands (HL<sub>n</sub>) were investigated. The thermogravimetric analysis of the compounds shows that the values of activation energies of decomposition ( $E_a$ ) are found to be 28.8, 25.7 and 40.0 kJ/mol for the ligands HL<sub>2</sub>, HL<sub>3</sub> and HL<sub>4</sub>, respectively, and the values of  $E_a$  are found to be 55.8, 38.9 and 69.1 kJ/mol for the complexes **2**, **3** and **4**, respectively. The calf thymus DNA binding activity of the ligands (HL<sub>n</sub>) was studied by absorption spectra measurements. The ligands considering that the —OH group may enhance their affinity towards DNA binding through formation of hydrogen bonding. The mechanism and the catalytic oxidation of benzylamine, and by *trans*-[Ru(L<sub>n</sub>)<sub>2</sub>(bipy)]Cl with hydrogen peroxide as co-oxidant were described.

## References

- [1] A.Z. El-Sonbati, A.A. El-Bindary, M.A. Diab, Sh.M. Morgan, Spectrochim. Acta A 135 (2015) 774–791.
- [2] A.Z. El-Sonbati, M.A. Diab, A.A. El-Bindary, G.G. Mohamed, Sh.M. Morgan, Inorg. Chim. Acta 430 (2015) 96–107.
- [3] A.Z. El-Sonbati, M.A. Diab, A.A. El-Bindary, Sh.M. Morgan, Spectrochim. Acta A 127 (2014) 310–328.
- [4] M.A. Diab, A.Z. El-Sonbati, A.A. El-Bindary, G.G. Mohamed, S.M. Morgan, Res. Chem. Intermed. (2015), <http://dx.doi.org/10.1007/s11164-015-1946-0>.
- [5] K. Hunger, Industrial Dyes. Chemistry, Properties, Applications, Wiley-VCH, Weinheim, 2003.
- [6] E.A.M. Geary, L.J. Yellowlees, L.A. Jack, I.D.H. Oswald, S. Parsons, N. Hirata, J.R. Durrant, N. Robertson, Inorg. Chem. 44 (2005) 242–250.
- [7] S. Bellotto, R. Reuter, C. Heinis, H.A. Wegner, J. Org. Chem. 76 (2011) 9826–9834.
- [8] H. Yousefi, A. Yahyazadeh, M.R. Yazdanbakhsh, M. Rassa, E.M. Rufchahi, J. Mol. Struct. 1015 (2012) 27–32.
- [9] N.H. Nataj, E. Mohajerani, H. Nemati, A. Moheghi, M.R. Yazdanbakhsh, M. Goli, A. Mohammadi, J. Appl. Polym. Sci. 127 (2013) 456–462.
- [10] A.A. Abdel Aziz, H.A. Elbadawy, Spectrochim. Acta A 124 (2014) 404–415.
- [11] A.A. Abou-Hussein, W. Linert, Spectrochim. Acta A 117 (2014) 763–771.
- [12] A.K. Pramanik, T.K. Mondal, Inorg. Chim. Acta 411 (2014) 106–112.
- [13] Y. Yamamoto, K. Fukatsu, H. Nishiyama, Chem. Commun. 48 (2012) 7985–7987.
- [14] A.F. El-Dessoki, A.F. Shoair, N.M. Hosny, J. Chem. Eng. Data 55 (2010) 267–272.
- [15] M. Hartmann, B.K. Keppler, Chem. Inorg. Chem. 16 (1995) 339–372.
- [16] G. Sava, S. Pacor, G. Mestroni, E. Alessio, Anticancer Res. 3 (1992) 25–31.
- [17] G. Sava, S. Pacor, G. Mestroni, E. Alessio, Clin. Exp. Metastasis 10 (1992) 273–280.
- [18] M. Plotek, R. Starosta, W. Nitek, U.K. Komarnicka, G. Stochel, A. Kyzioł, Polyhedron 68 (2014) 357–364.
- [19] U. McDonnell, M.R. Hicks, M.J. Hannon, A. Rodger, J. Inorg. Biochem. 102 (2008) 2052–2059.
- [20] M. Shebl, Spectrochim. Acta A 117 (2014) 127–137.
- [21] N.A. El-Ghamaz, M.A. Diab, A.A. El-Bindary, A.Z. El-Sonbati, H.A. Seyam, Mater. Sci. Semicond. Proc. 27 (2014) 521–531.
- [22] A.F. Shoair, A.R. El-Shobaky, E.A. Azab, J. Mol. Liq. 203 (2015) 59–65.
- [23] A.F. Shoair, A.A. El-Bindary, Spectrochim. Acta A 131 (2014) 490–496.
- [24] M.J. Waring, J. Mol. Biol. 13 (1965) 269–282.
- [25] M.F. Reichmann, C.A. Rice, C.A. Thomas, P. Doty, J. Am. Chem. Soc. 76 (1954) 3047–3053.
- [26] A. Wolfe, G.H. Shimer, T. Meehan, Biochem. 26 (1987) 6392–6396.
- [27] J. Zhu, P.C. Wang, M. Lu, Appl. Catal. A: General 477 (2014) 125–131.
- [28] J. Geary, Coord. Chem. Rev. 7 (1971) 81–122.
- [29] F.A. Cotton, C.W. Wilkinson, Advanced Inorganic Chemistry, 3rd Ed. Interscience Publisher, New York, 1972.
- [30] K. Nakamoto, Infrared and Raman Spectra of Inorganic and Coordination Compounds, Wiley-Interscience, New York, 1971.
- [31] A.Z. El-Sonbati, Spectroscopy Lett. 30 (1997) 459–462.
- [32] A.A. El-Bindary, Transition Met. Chem. 22 (1997) 381–384.
- [33] I. Masih, N. Fahmi, Spectrochim. Acta A 79 (2011) 940–947.
- [34] A.Z. El-Sonbati, M.A. Diab, M.M. El-Halawany, N.E. Salam, Met. Chem. Phys. 123 (2010) 439–449.
- [35] J. Ladić, A. Messumer, J. Redly, Acta Chim. Acad. Sci. Hung. 38 (1963) 393–397.
- [36] M.A. Diab, A.A. El-Bindary, A.Z. El-Sonbati, O.L. Salem, J. Mol. Struct. 1007 (2012) 11–19.
- [37] A.Z. El-Sonbati, M.A. Diab, M.M. El-Halawany, N.E. Salam, Spectrochim. Acta A 77 (2010) 795–801.
- [38] N.A. El-Ghamaz, A.Z. El-Sonbati, M.A. Diab, A.A. El-Bindary, M.K. Awad, Sh.M. Morgan, Mater. Sci. Semicond. Proc. 19 (2014) 150–162.
- [39] A.W. Coats, J.P. Redfern, Nature 20 (1964) 68–79.
- [40] H.W. Horowitz, G. Metzger, Anal. Chem. 35 (1963) 1464–1468.
- [41] J.M. Chen, W. Wei, W.X.L. Feng, T.B. Lu, Chem. Asian J. 2 (2007) 710–714.
- [42] J.P. Costes, F. Dahan, J.P. Laurent, M. Drillon, Inorg. Chem. Acta 294 (1999) 8–12.
- [43] N. Miyaura, Synlett 13 (2009) 2039–2050.
- [44] J.S.M. Samec, A.H. Ell, J.E. Backvall, Chem. Eur. J. 11 (2005) 2327–2334.
- [45] F. Li, J. Chen, Q. Zhang, Y. Wang, Green Chem. 10 (2008) 553–562.
- [46] N. Gunasekaran, R. Karvembu, Inorg. Chem. Commun. 13 (2010) 952–955.
- [47] S. Priyarega, M.M. Tamizh, R. Karvembu, R. Prabhakaran, K. Natarajan, J. Chem. Sci. 123 (2011) 319–325.